PCCP

The physical conditions for UO formation in laser-produced uranium plumes

Journal:	*Physical Chemistry Chemical Physics*
Manuscript ID	CP-ART-04-2019-002250.R2
Article Type:	Paper
Date Submitted by the Author:	20-Jun-2019
Complete List of Authors:	Harilal, Sivanandan; Pacific Northwest National Laboratory, National Security Directorate Kautz, Elizabeth; Pacific Northwest National Laboratory, National Security Directorate Bernacki, Bruce; Pacific Northwest National Laboratory, National Security Directorate Phillips, Mark; University of Arizona, Optics Science Center; Opticslah, LLC; Pacific Northwest National Laboratory, National Security Directorate Skrodzki, Patrick; University of Michigan, Nuclear Engineering and Radiological Sciences; University of Michigan, Center for Ultrafast Optical Science Burger, Milos; University of Michigan, Nuclear Engineering and Radiological Sciences; University of Michigan, Center for Ultrafast Optical Science Jovanovic, Igor; University of Michigan; University of Michigan, Center for Ultrafast Optical Science

ARTICLE

The physical conditions for UO formation in laser-produced uranium plumes

Received 00th January 20xx,
Accepted 00th January 20xx

DOI: 10.1039/x0xx00000x

S.S. Harilal,[a]* E.J. Kautz, [a] B.E. Bernacki, [a] M.C. Phillips, [a,b,c] P.J. Skrodzki, [d,e] M. Burger, [d,e] I. Jovanovic[d,e]

We investigate the oxidation of uranium (U) species, the physical conditions leading to uranium monoxide (UO) formation and the interplay between plume hydrodynamics and plasma chemistry in a laser-produced U plasma. Plasmas are produced by ablation of metallic U using nanosecond laser pulses. An ambient gas environment with varying oxygen partial pressures in 100 Torr inert Ar gas is used for controlling the plasma oxidation chemistry. Optical emission spectroscopic analysis of U atomic and monoxide species shows a reduction of the emission intensity and persistence with increasing oxygen partial pressure. Spectral modelling is used for identifying the physical conditions in the plasma that favor UO formation. The optimal temperature for UO formation is found to be in the temperature range of ~1500–5000 K. The spectrally-integrated and spectrally-filtered (monochromatic) imaging of U atomic and molecular species reveal the evolutionary paths of various species in the plasma. Our results also highlight that oxidation in U plasmas predominantly happens at the cooler periphery, and is delayed with respect to plasma formation, and the dissipation of molecular species strongly depends on oxygen partial pressure.

1. Introduction

Laser-induced breakdown spectroscopy (LIBS) is a valuable analytical technique for detection of various elements including special nuclear materials.[1] The major advantages of LIBS compared to other analytical tools are real-time detection, no requirement for sample preparation, and standoff measurement capability [2]. LIBS needs only optical access to the sample, and the standoff distance is governed by the laser focusing conditions as well as the return light collection efficiency. Although LIBS has been used routinely for the analysis of low-Z materials[3-6] for a variety of applications (e.g. geochemistry, combustion, forensics, biomedical)[7], there exist certain challenges for using LIBS for analysing high-Z materials, such as uranium (U) or other actinides. LIBS of a U-containing target provides very congested spectral features, with approximately ~10^5 lines in the UV-visible spectral range originating from ~1600 energy levels.[8-10] Thus, accurate identification of various atomic transitions as well as quantification is always problematic even with the use of high-resolution spectrographs.[2, 11]

It is well known that U oxidizes rapidly in an oxygen-containing high-temperature environment.[11-13] For example, the oxygen present in the air reacts rapidly with U species in the plasma leading to uranium oxide formation (U_xO_y). Hence the emission from UO and higher oxide molecular bands from the plasma plume complicates the already congested atomic spectral features of U. Therefore, understanding the molecular formation through plasma and thermochemistry in U plumes is very important for numerous fields including forensic analysis, environmental monitoring, U nucleation physics, and debris analysis in a weapons detonation event, or reactor accident scenario. Motivated by this broad applicability, several studies have focused on understanding plasma chemistry in U plumes, as well as identifying spectral features of UO and higher oxides from laser ablation plumes.[11-22] Additionally, the thermodynamics leading to molecular and nanocluster formation in a laser-produced plasma still remains a mystery, and considerable efforts are ongoing to improve understanding of the evolutionary paths of molecules and condensed nanoparticles and their relation to laser-plume hydrodynamics.[23-26]

Among the various plasma diagnostic tools, optical emission spectroscopy is a versatile tool providing information about the composition of the plasma as well as the plume fundamentals such as density, and temperature with reasonable accuracy.[27] However, the inter-related hydrodynamics and chemistry in the plasma affect the emission features. Fast-gated imaging using narrow-band filters (monochromatic imaging) offers another dimension to plasma diagnostics by providing time-resolved hydrodynamic expansion features of the plume as well as spatial locations of the oxidation/combustion in the plasma.[26] Our recent studies showed that the spectral features of U-containing plasmas formed in air include a strong background, where a high spectral density of overlapping lines from various U_xO_y compounds provides a significant contribution.[17] Spatio-

[a.] Pacific Northwest National Laboratory, Richland, WA 99352 USA
[b.] Optics Science Center, University of Arizona, Tucson, AZ 85721 USA
[c.] Opticslah, LLC, 2350 Alamo Ave. SE, Albuquerque, NM 87106 USA
[d.] Department of Nuclear Engineering and Radiological Sciences, University of Michigan, MI 48109 USA
[e.] Center for Ultrafast Optical Science, University of Michigan, MI 48109 USA
*Corresponding Author Email: hari@pnnl.gov
DOI: 10.1039/x0xx00000x

temporal mapping of U plasma employing optical emission spectroscopy in the oxygen-rich environment showed a reduction in emission persistence from both U atoms and UO molecules with the formation of uranium higher oxides (U_xO_y).[15] The present studies explore spatially-integrated and time-resolved emission features of U plasma as a function of varying oxygen partial pressures, from 1% to 20% O_2. Such spatially integrated self-emission analysis is a prerequisite for any standoff measurement of U ablation plumes.[2, 28] The physical conditions of the plasma that favour UO molecular formation are evaluated by comparing the measured spectral features with spectral simulation. We also report time and spectrally resolved 2D monochromatic imaging to compare differences in plume morphology and emission characteristics for a subset of the oxygen partial pressures studied here. Monochromatic imaging of the plume combined with simulated and measured spectral features provides a unique insight into the fundamentals of U oxidation in a high-temperature plasma/fireball environment. Our studies show that the oxidation reactions in the U plasma predominantly occurs at the plume periphery where plasma temperatures are lower and the plume hydrodynamics is greatly influenced by the oxygen concentration in the ambient environment.

2. Experimental

For producing plasmas, the 1064 nm fundamental radiation from an Nd:YAG laser with 6 ns full width half maximum (FWHM) was focused on a natural U metal using an f/15 antireflection coated plano-convex lens. The natural U target analysed has an enrichment level of 0.7% ^{235}U, where enrichment is defined as the atomic fraction of ^{235}U relative to all U isotopes. The spot size and laser fluence at the target surface were ~1 mm and ~12 J/cm^2 (intensity ~2 GW/cm^2), respectively. The target was mounted in a 6" cube-shaped vacuum chamber evacuated by a dry pump which provided a base pressure of ~5 mTorr. The chamber possesses optical windows for laser ablation, light collection and vacuum ports for pumping, gas feedthrough, and pressure gauge. A custom-built gas-line manifold which contained several stages of leak valves and regulators was used for filling gases with appropriate concentrations and partial pressures in the chamber. The gas feedthrough port was connected to a gas manifold so that the composition and pressure of the gas could be easily varied. The chamber was mounted on an *x-y-z* translator which was moved to avoid target cratering effects.

For optical emission spectroscopy, the light emitted from the plasma was collected approximately normal to the U target surface using a convex lens and focused on to a 400 µm multimode fiber. Thus, the emission measurements were performed in a space-integrated manner, but such a light collection scheme is essential for any standoff LIBS experiments. The fiber was coupled to a 0.5 m triple-grating spectrograph. The spectra were recorded using a 500 nm blazed 2400 grooves/mm grating. The measured instrumental linewidth using a He-Ne laser was ~35 pm. The wavelength calibration of the spectrograph was performed using Hg lamp as well as U spectral lines. An intensified charged coupled device (ICCD, 1024 ×1024 pixels) was used for recording the wavelength dispersed light. The ICCD was synchronized with laser pulse using a timing generator and the acquisition gate delay and the integration time were varied for time-resolved measurements. Another ICCD camera was used for imaging the self-emission and the hydrodynamic expansion of the U plasma. For this, an objective was used for collecting and imaging the self-emission from the plasma onto the intensifier of the ICCD. The spectrally-integrated images were collected for evaluating plume hydrodynamics, while narrowband filters centered at 404 nm and 593.50 nm were used for capturing the emission zones of U atomic and UO molecular species within the plasma, respectively.

3. Results and Discussion

3.1. UO Spectroscopy

All spectroscopic measurements were performed at 100 Torr pressure, where oxygen partial pressures (PP) are varied in the range of 1–20% in an inert Ar ambient. The corresponding oxygen concentration in the chamber was from 3.2×10^{16} to 6.4×10^{17} cm^{-3}. The use of Ar as the other component of the gas environment when varying the oxygen PPs eliminates all reaction routes except U oxidation/combustion. Since a 100 Torr pressure level is used for all measurements, the anticipated plume confinement effects are similar for all oxygen PPs when considering the negligible difference in the mass of Ar and O_2. Previous studies also showed that the ns LIBS plumes provide the highest signal to noise ratio (SNR) at ~100 Torr pressure levels.[29] The oxide molecular species in the U plasma are formed through interaction with ambient O_2 (combustion) and/or through interacting with impurity oxygen from the sample. The oxidation of the U metal sample is unavoidable during target loading in the chamber. Before collecting U spectral data, we applied several cleaning laser shots to the target for removing the oxide layer.[17] For this reason, it can be concluded that the major reason for oxidation in the present experiment is due to interaction with oxygen molecules from the cover gas.

The congested spectral features of U is well documented in the literature [8,11,17,30-34]. For resolving U transitions, extremely high-resolution spectrographs are needed for overcoming instrumental broadening seen in emission spectroscopy. Laser spectroscopy tools such as laser-absorption spectroscopy and laser-induced fluorescence, which are immune to instrumental broadening, are capable of resolving spectral features of U without negligible overlapping[2, 35, 36]. Typically, the emission from atoms and ions predominate at the earliest times in the evolution of the LPP while the molecular emission appears at later times.[2] However, the time scales for their appearance will change significantly with initial conditions in the plasma. For example, the molecular emission appeared at delayed times ~ 10 µs for ns LIBS, while it may co-exist at the early times with atomic emission in the case of fs and filament LIBS.[2] The delayed molecular emission in ns laser-produced plasmas was

explained due to the presence of strong shock waves which act a barrier between plume and ambient[26] and existence of higher temperatures at the early times of ns laser-produced plasma.

For studying U atomic and molecular emission features, we monitored the spectral features in the wavelength range 591–595 nm, where emission from U atoms, UO, and U_xO_y species coexist.[11, 15, 17] Figure 1 gives time-resolved and space-integrated emission features of atomic U and UO for 1%, 2%, and 5% O_2 PPs; in Figure 2, the spectral features obtained with 10% and 20% O_2 PPs are given. The major UO feature in the spectra is a band centered at 593.55 nm. The other spectral features seen in the figures are due to U I emission and the most noticeable among them are a resonance transition at 591.54 nm (0–16900 cm^{-1}) and a near-resonance line at 593.38 nm (620–17468 cm^{-1}). The other prominent lines of U I that appear in the spectral widow are also marked in Figure 1 and they originate from higher excited levels: 592.55 nm (7646–24517 cm^{-1}); 592.93 nm (3801–20662 cm^{-1}); 594.28 nm (5762–22585 cm^{-1}); and 594.86 nm (7646–24452 cm^{-1})). The U I lines with higher upper energy levels can only be seen at early times of plasma evolution, while the transitions coupled to the ground state or near ground state can be seen even at very late times along with the emission from molecular species. This can be understood by considering the relation of the excited state population of U atomic species to the temperature of the plasma system through Boltzmann equation, assuming local thermodynamic equilibrium (LTE). The other spectral features due to oxides can also be seen at later times marked as U_xO_y in Figure 1a. [17] Previous reports show that the temperature of LPP decays exponentially with time.[37] In an LPP the emission from atoms dominates at early times of its evolution when the temperature of the system is higher, while the molecular spectral features appear when the physical conditions of the plasma are cooler.[2, 21] Although the spectral measurements presented in this work are space-integrated, it should also be mentioned that the temperature of a LPP system also varies significantly with distance from the target.[2]

Regardless of oxygen PPs used, as shown in Figures 1 and 2, the emission from U I dominates at early times, while UO emission becomes predominant at later stages of plasma evolution, although the temporal history and persistence change with varying oxygen concentrations. At lower oxygen partial pressures (*e.g.* 1%), the atomic and molecular spectral features persist up to ~ 70 µs. However, emission persistence is considerably reduced with increasing oxygen concentration. For example, at 5% oxygen PP, the persistence of emission from the plasma is found to be ~60 µs, while the emission persistence is reduced to ~30 µs and ~20 µs for 10 % and 20% oxygen PPs, respectively. The spectral features also show that the appearance of UO emission occurs at early times with increasing oxygen concentration with an overall reduction in emission persistence for both U and UO. Our previous studies showed that at higher O_2 concentrations, the polyatomic oxides (UO_2, U_xO_y, etc.) will form[15], eventually depleting the population of both U atoms and UO molecules. The polyatomic oxides typically provide broadband emission, which is evidenced by the existence of '*background-like*' emission in the spectral features given in Figures 2 and 3. Another interesting observation from the spectral features of U and UO are the changes in their relative intensity at various O_2 PPs. At 1% O_2 PP, the UO emission is found to be more intense than U I emission peak at 591.54 nm at late times. However, at higher O_2 PPs the UO emission intensity is always weaker compared to U I, even at late times in the plasma evolution.

Figures 1 and 2 also show that the spectral features measured at ≤ 5 µs are similar for all oxygen PPs and are dominated by U I lines. This indicates that at early times of plume evolution the temperature of the plasma system is not favourable for the molecular formation. In addition, at early times of plasma expansion, the interaction between the plume and oxygen species may be limited because of the presence of strong shock waves.[26] For a direct comparison, the spectral emission measured at 5 µs and 10 µs delays for various oxygen concentrations is shown in Figure 3. The spectral features recorded at 5 µs delay show an increasing intensity for UO peak with oxygen concentration (dotted line in Figure 3a). However, significant changes in the spectral features can be seen as the delay increases to 10 µs. At 10 µs delay and at lower oxygen partial pressures, the spectral features are dominated by U I line, whereas UO and U_xO_y dominate at higher oxygen partial pressures. These results highlight that, increasing oxygen partial pressures lead to earlier molecular formation in U plasma.

The results presented in Figures 1 and 2 provide evidence that the O_2 partial pressures influence the plasma physical and chemical conditions, which in turn affect the temporal evolution of U spectral features and its persistence. Previous studies showed that the persistence of U ground state and excited populations are greatly affected by the presence of air, when compared to inert nitrogen or argon ambient.[19, 38] It is therefore interesting to examine the time evolution of emission from selected transitions of U atoms and UO molecules for varying oxygen partial pressures. The time dependence of U I at 591.54 nm and UO at 593.55 nm is presented in Figure 4. Temporal decay of emission from both species is found to be minimal when the oxygen PP is increased from 1% to 2%, but a sharp decay in intensity and hence persistence can be seen when the O_2 PP is raised to 5% or higher. An enhancement in the UO emission is also evident at 5% O_2 PP up to ~30 µs relative to lower oxygen PPs. Figure 5a shows the time evolution of the ratio of the peak intensities of UO 593.55 nm and U I emission at 591.54 nm, which is useful for the understanding the formation and dissipation of U diatoms in the plasma. In all O_2 PPs studied, the UO/U ratio increases rapidly with time; however, a sharper increase can be seen for higher O_2 PPs. This could be related to the greater availability of oxygen molecules in the ambient for oxidation. At 1% O_2 PP, the UO peak emission is found to be stronger than U at times ≥50 µs. For 2% O_2 PP, the intensity ratio achieves unity and then levels off at later times. A similar trend can also be seen for 5% O_2 PP although the reduction or leveling off the intensity ratio happens at early times. For 10% and 20% O_2 PPs, the persistence of plasma is significantly reduced and the leveling off the intensity ratio is not apparent.

A previous study employing fs laser ablation of U in 1-atm air showed that the ratio of UO emission over the U I emission was higher than unity at later times of plasma evolution, indicating that molecular emission predominates in the fs LPP emission spectrum compared to ns LPP.[11] However, it has to be noted that the molecular-to-atomic emission intensity ratio depends strongly on the line selection as well as physical conditions exist in the plasma plume. In the fs LPP studies the ratio was calculated using U I at 593.38 nm, which is relatively a weak transition (transition probability A=1.3x10^5 s^{-1}; 620–17468 cm^{-1}) compared to the U I resonance transition at 591.54 nm (A= 9.5x10^5 s^{-1}; 0–16900 cm^{-1}) used in Figure 5a. For a direct comparison, the ratio of emission intensities of UO 593.55 nm to U I 593.38 nm is given in Figure 5b, which shows similar trends, although intensity ratios are significantly higher, especially for higher O_2 PPs. The saturation of intensity ratio is also evident in this scenario for lower O_2 PP. Therefore, the plots given in Figure 5 imply that a caution must be observed when correlating the molecular atomic intensity ratios to physical conditions of the plume. The increase and reduction or saturation of UO to U intensity ratio show the creation and dissipation of UO molecules in the plasma with varying O_2 PPs. The saturation of intensity ratio of UO to U at late times of plasma evolution in oxygen-rich ambient can be related to the formation of U polyatomic oxides (U_xO_y). According to uranium oxidation chemistry, UO acts as a precursor for forming higher oxides.[14]

The oxidation in a laser-produced plasma occurs when the temperature of the plasma is low and sufficient density of oxygen is present, such that favourable physical conditions exist for the generation of molecules. Considering the fact that similar conditions were present in all measurements, except for the changes in O_2 PPs, it can be concluded that plasma chemistry is the major reason for the reduction in emission intensity and persistence of all species in the plume. Previous studies showed that in 1-atm ambient, the oxidation/combustion of Al plume is delayed by the presence of shock waves.[26] However, the strength of the shock waves is significantly weaker at 100 Torr compared to 1-atm ambient, as evidenced by low contrast in recorded shadowgrams.[39] Therefore, the occurrence of UO molecules at early times of plasma evolution when the O_2 PP is increased can be related to oxygen diffusion into the plume and/or oxidation in the plume-ambient boundary. From a diagnostics point of view, 2D gated and monochromatic images of U and UO will be useful for studying the oxidation processes in U plasma.

3.2 Spectral Modelling and Temperature Evaluation

The spectral features recorded from U plasma can be used for measuring the temperatures of the plasma system by comparison with simulated spectra. The Palmer Atlas data[8] shows 53 transitions of U in the spectral range of 591–597 nm, which includes 41 U neutral transitions, 2 singly ionized U transitions (U II), and 10 transitions for which energy levels are not identified. Figure 6 shows a comparison of experimentally recorded spectra with simulated spectra at various temperatures. The modelled spectra used a U number density of N = 1×10^{15} cm^{-3}, a length of the slab L= 1 cm, and assumed homogeneous conditions along the slab. Doppler broadening was calculated analytically, and van der Waals broadening was approximated at a pressure of 100 Torr to be ~1.6 pm. The modelled spectra were convolved with a Lorentzian instrument function with 35 pm FWHM, corresponding to the spectrograph resolution. Self-absorption is included in the model, and comparison with spectra at different U number densities and slab lengths indicates some lines are self-absorbed. Radiative transport effects due to spatially-varying physical conditions, such as self-reversal, are not included in the modelled spectra. The accuracy of the relative oscillator strength is ±20% and the 10 transitions listed in the Palmer Atlas with unidentified energy levels were not included because their scaling with excitation temperature is unknown. The presence of oxygen generates U_xO_y spectral features which are not accounted for. Nevertheless, the measured and simulated U spectra show good agreement. Hence, despite the identified limitations of the spectral model, it is a useful tool for measuring the average temperature of the plasma system.

The estimated temperature of the plasma system by comparing the recorded spectral details at various O_2 PPs with simulated ones are given in Figure 7. For estimating temperature, we compared the line intensities emanated from higher excitation levels for early times and used resonance or near resonance lines at very late times of plasma evolution. The uncertainty is dominated by spatial and temporal gradients in the plasmas, variations in optical thickness, and that the temperature determined is at best a weighted average along the line-of-sight of the measurement. The estimated excitation temperature at early times of plasma evolution is similar (7000 ± 500 K) for all O_2 PPs and it decreases with time; however, the temperature decays more rapidly for increasing O_2 PPs. For example, the temperature of the plasma at ~20 µs is ~4000 K for 1% O_2 PP, while at the same delay the temperature is found to be significantly lower for higher O_2 PP (~2500 K for 5% O_2 PP and ~1500K for 10% O_2 PP, respectively). By comparing the spectral features and estimated temperatures it can be concluded that the UO formation is favoured in the temperature range ~1500–5000 K assuming U and UO species co-located in the plasma. These temperatures agree well with predicted temperatures of UO formation in U plasma through modeling.[21] Regardless of the O_2 PPs, the UO emission is present along with other broad higher oxide (U_xO_y) peaks at later times of the plasma evolution; however, the U I emission lines are found to be weak for temperature analysis. The U oxidation process is exothermic, but a temperature increase with time due to reactive heating is not evident in Figure 7. It should be mentioned that the thermodynamics of U ablation plume is changing rapidly with time and space from the target. The spectral measurements given here are performed in a space-integrated manner and hence it is not possible to see any localized effects; however, monochromatic imaging of U and UO, which is discussed below, is useful for providing valuable insight in this context.

3.3. Monochromatic Imaging of U and UO

Fast-gated and spectrally-integrated imaging employing an ICCD has been extensively utilized for understanding the hydrodynamics of the LPP systems at all pressure levels. Such 2D gated images of the expanding LPP plumes provide shape and velocity of the plume, distribution of various species, shock dynamics, internal structures and instabilities.[40-42] We recorded spectrally-integrated (350–800 nm) and spectrally-resolved images for analyzing the overall self-emission features as well as the spatial locations of excited U atoms and UO molecules in the plasma at various times and O_2 PPs. For analyzing emission from U atoms and molecules, two narrowband filters were used. For collecting UO emission, a narrowband filter having peak transmission at 593.5 nm with 0.18 nm FWHM was used. Due to the spectral congestion, it is anticipated that the UO spectral images may contain radiation from UI 593.38 nm at early times. However, at later times, based on results presented in Figures 1 and 2, it can be concluded that the recorded self-emission from the plasma is primarily due to UO. For recording 2D imaging of U atomic emission, a narrowband filter centered at 404 nm with a 1 nm FWHM was used. The images collected using this filter may contain emission predominantly from U I (5 lines) and U II (one line). The predominant lines which exist in the filter transmission range are U I emission at 403.67 nm (3800–28566 cm^{-1}), 403.8 nm (4275–29033 cm^{-1}), 403.97 nm (7646–32393 cm^{-1}), 404.07 nm (0–24741 cm^{-1}), and 404.27 nm (620–25349 cm^{-1}), and U II at 404.44 nm (5260-29978 cm^{-1}). However, the ionic emission in a laser plasma typically exists at early times of its evolution, when the temperatures are in the excess of ~1 eV. Hence, the filtered images recorded at later times of plasma evolution are likely due to U I emission.

Figure 8 gives the time evolution of spectrally integrated (SI), and monochromatic self-emission images of U atoms and UO molecules for two oxygen PPs, *viz.* 1% and 20%. Since the plume images were recorded at the relatively high-pressure background (100 Torr), the shot to shot fluctuation due to the presence of instabilities cannot be avoided. Our measurement showed that the shot to shot fluctuations in the total intensity counts was less than 8 %. Please note that the time scales given for Figure 8 (a) and (b) are different for 1% and 20% O_2 PPs due to the difference in persistence of U plasma. The persistence of U plasma in 1% oxygen PP is found to be ≥60 μs, while it is reduced to ~20 μs at 20% O_2 PP. To better interpret and analyse images of U plasmas, raw grayscale image data was processed by stretching image contrast, sharpening the image with high boost filtering, and by applying jet colour map to visualize the plasma plume in a more dynamic colour scheme. To account for large differences in absolute emission, image intensities are scaled for each image individually between 0 and 1, as indicated by the colour scale in Figure 8. The spectrally-integrated images in the wavelength range of 350–900 nm represent overall plume morphology. The temporal duration of integration for obtaining the images is listed in Figure 8 caption.

Compared to the free expansion of the plume in a vacuum or low-pressure levels, the images given in Figure 8 show strong confinement effects.[43] The contribution from plume confinement effects is anticipated to be similar with varying oxygen concentrations in 100 Torr Ar backup pressure level considering the small differences in the mass of the gases used (m_{Ar} = 40 amu and m_{O2} = 32 amu) and the lesser mole fractions of O_2 (1–20%). However, significant differences in plume morphology and persistence can be seen when the oxygen PPs increases from 1 % to 20%, and this could be attributed to U oxidation thermo- and plasma chemistry. Regardless of the oxygen concentrations, the role of oxidation chemistry is limited at very early times of plume's lifetime, where hotter conditions exist. Comparing the spectrally integrated images with U and UO at 1% O_2 PP (Figure 8a), it can be concluded that UO is formed at the outer layers of the plume, where cooler conditions exist. At later times (1% O_2 PP, ~60 μs) UO formation is also evident closer to the target, which could be caused by the diffusion of the oxygen molecules as well as the existence of cooler temperature near to the target surface at later times.

In the 20% O_2 PP case (Figure 8b), the persistence of the plasma is limited to early times because of oxygen-assisted chemistry. Several emission 'hot spots' exist in the images recorded with higher oxygen concentrations. When a U plasma expands in an oxygen-rich environment, the ablation plume morphology is controlled not only by the local temperature, but also by the availability of oxygen for the reaction chemistry. Because of the differences in plume persistence, a direct comparison of images is challenging throughout the plasma evolution, but is possible at 10 μs delay. Based on the spectral features given in Figure 3b (10 μs delay), the emission from U atoms predominates when the O_2 PP is 1%, while the emission from U_xO_y prevails when the O_2 PP is increased to 20%. Comparing the plume morphologies, the center of mass of the UO emission zone is shifted to plume front when the O_2 PP is increased to 20%, which indicates U gas-phase oxidation is primarily happening at the plume edges. In the 1% O_2 PP and at ~10 μs, the spectrally filtered (monochromatic) emission of UO may also contain U I from the nearly 593.38 nm line; however, at 20% O_2 PP the UO image may be entirely due to U_xO_y emission. The monochromatic imaging of U and UO shows segregation in space. But, the spectral features given in Figures 1-3 are spatially integrated and used to estimate an average plasma temperature. Based on the imaging results, the U and UO emission originate from different parts of the plasma, which may have different temperatures. The spatially integrated spectral features are used for measuring the temperature by comparing with simulated spectra; therefore, the excitation temperature given in Figure 7 should be considered as an average temperature of the plasma system.

Predicting reaction pathways for U_xO_y formation in a thermodynamically controlled system is a complex process. Even a well-characterized U plasma-chemical system that includes oxygen may contain a large number of reaction routes. The situation becomes extremely challenging for a laser-produced plasma system where large gradients in plume temperature, pressure, and number density of U-containing particles exist with time and space. Finko *et al.*[14, 21] listed some of the most favourable thermochemistry (12 channels) and plasma chemistry (17 channels) reaction pathways for the

formation of U_xO_y. In addition to these, the electron impact dissociation, excitation, and ionization of ambient oxygen atoms/molecules may exist in the system. Based on the images, the uranium atomic concentration is higher closer to the target compared to the edges, where the formation of oxides reduces its number density. Some of the potential reaction routes involving U atoms include $U + O_2 \leftrightarrows UO + O$; $U+O_2 \leftrightarrows UO_2$ *etc.* The concentration of UO near the target at early times depends on the availability of the oxygen within the plume. Similarly, the concentration of UO is diminished at the outer edges of the plume due to the formation of higher oxides by consuming UO and the potential reaction routes include $UO + O \leftrightarrows UO_2$, $UO+O_2 \leftrightarrows UO_2 + O$; $UO + O_2 \leftrightarrows UO_3$; $UO + UO \leftrightarrows U_2O_2$; $UO + UO_2 \leftrightarrows U_2O_3$, *etc*. At early times, because of the high plume particle density and/or presence of shock waves, the oxidation will be limited only at the plume edges, but at later times, the diffusion of the oxygen molecules into the plasma system leads to oxide formation closer to the target. The turbulent transport of high-Z plasma in a low-Z ambient medium, which is caused by the presence of instabilities such as Rayleigh-Taylor and Richtmyer-Meshkov near the plume edges, may also help for mixing of the ambient and the plume species at late times in the plasma evolution.

4. Conclusions

The gas-phase oxidation of U plasma was evaluated in a laser-produced plasma system employing emission spectroscopy and 2D monochromatic imaging. For controlling the U plasma chemistry, the oxygen partial pressure was varied in the range of 1–20% in an Ar backup gas. Optical emission spectroscopic analysis of U atomic and UO molecular species showed a significant reduction in the emission intensity and persistence when the oxygen partial pressures are increased from 1 to 20% O_2. The spectral features also showed that the emission from U I arising from various excitation levels dominates at early times of plume evolution, while UO emission and U I resonance transitions become predominant at later stages of plasma evolution although their temporal history and persistence change with varying oxygen concentrations. For example, the emission from the atomic and molecular spectral features persist $\gtrsim$ 70 μs for 1% O_2 PP, while the emission persistence is reduced to ~20 μs for 20% O_2 PP. The spectral features also show that the appearance of UO emission occurs at early times with increasing oxygen concentration with an overall reduction in emission persistence for both U and UO. The intensity ratios of UO/U at various O_2 PPs indicate the creation and dissipation of U oxides in the plasma. The saturation of intensity ratio of UO to U at late times of plasma evolution at oxygen-rich ambient is due to the formation of U polyatomic oxides (U_xO_y).

The physical conditions of the plasma were determined by comparing the simulated and measured U I spectral features. The measured temperature show a rapid reduction with increasing oxygen partial pressure, although initial plasma conditions are similar. By comparing the recorded and simulated spectral features, the favoured physical conditions for UO formation occur in the temperature range 1500–5000 K under the assumption that U and UO co-exist in the plasma. However, a comparison between spectrally-integrated self-emission from the U plasma and monochromatic imaging of U atoms and UO molecules highlighted that the oxidation of the plume primarily occurs at the plume front. Therefore, caution must be taken when using the physical conditions of the plasma derived from the spectral modelling to predict the favourable conditions of molecular formation in U plasma. A comparison of the measured and modelled UO spectral features is essential for addressing this issue. The results obtained from the monochromatic images also show a complex interplay between plume expansion, thermochemistry, and plasma chemistry.

Conflicts of interest

There are no conflicts to declare.

Acknowledgements

The authors acknowledge the following agencies for financial support for this work: the U.S. Department of Energy/National Nuclear Security Administration (DOE/NNSA) Office of Nonproliferation and Verification Research and Development (NA-22), and the Consortium for Verification Technology under Department of Energy National Nuclear Security Administration (DE- NA0002534). PJ Skrodzki acknowledges the National Science Foundation for a Graduate Research Fellowship (DGE 1256260). The work presented here was performed at Pacific Northwest National Laboratory which is operated for the U.S. DOE by Battelle Memorial Institute under Contract No. DE-AC05-76RLO1830.

References

1. S. Musazzi and U. Perini, *Laser-Induced Breakdown Spectroscopy – Fundamentals and Applications* Springer Series in Optical Sciences, 2014.
2. S. S. Harilal, B. E. Brumfield, N. L. LaHaye, K. C. Hartig and M. C. Phillips, *Applied Physics Reviews*, 2018, **5**, 021301.
3. Y. Wang, A. M. Chen, L. Z. Sui, S. Y. Li, D. L. Liu, X. W. Wang, Y. F. Jiang, X. R. Huang and M. X. Jin, *Physics of Plasmas*, 2016, **23**, 113105.
4. L. St-Onge, M. Sabsabi and P. Cielo, *J. Anal. Atom. Spectrosc.*, 1997, **12**, 997-1004.
5. J. S. Cowpe, J. S. Astin, R. D. Pilkington and A. E. Hill, *Spectrochimica Acta Part B: Atomic Spectroscopy*, 2008, **63**, 1066-1071.
6. F. Colao, V. Lazic, R. Fantoni and S. Pershin, *Spectrochim. Acta Part B*, 2002, **57**, 1167-1179.
7. D. W. Hahn and N. Omenetto, *Applied Spectroscopy*, 2012, **66**, 347-419.
8. B. A. Palmer, R. A. Keller and J. R. Engleman, *An Atlas of Uranium Emission Intensities in a Hollow Cathode Discharge*, Report LA-8251-MS, Los Alamos Scientific Laboratory, 1980.
9. J. Blaise, J.-F. Wyart, J. Vergès, R. Engleman, Jr.j, B. A. Palmer and L. J. Radziemski, *J. Opt. Soc. Am. B*, 1994, **11**, 1897-1929.

10. J. Blaise and L. J. Radziemski, Jr., *J. Opt. Soc. Am.*, 1976, **66**, 644-659.
11. K. Hartig, S. S. Harilal, M. C. Phillips, B. E. Brumfield and I. Jovanovic, *Optics Express*, 2017, **25** 11477-11490.
12. T. L. Martin, C. Coe, P. A. J. Bagot, P. Morrall, G. D. W. Smith, T. Scott and M. P. Moody, *Sci Rep-Uk*, 2016, **6**, 25618.
13. L. Kaledin and M. Heaven, Journal of Molecular Spectroscopy 1997, 185, 1-7.
14. M. S. Finko, D. Curreli, D. G. Weisz, J. C. Crowhurst, T. P. Rose, B. Koroglu, H. B. Radousky and M. R. Armstrong, *Journal of Physics D-Applied Physics*, 2017, **50**, 485201.
15. P. Skrodzki, M. Burger, I. Jovanovic, B. E. Brumfield, M. C. Phillips and S. S. Harilal, *Optics Letters*, 2018, **43**, 5118.
16. D. G. Weisz, J. C. Crowhurst, W. J. Siekhaus, T. P. Rose, B. Koroglu, H. B. Radousky, J. M. Zaug, M. R. Armstrong, B. H. Isselhardt, M. K. Savina, M. Azer, M. S. Finko and D. Curreli, *Applied Physics Letters*, 2017, **111**, 034101.
17. S. S. Harilal, B. E. Brumfield, N. Glumac and M. C. Phillips, *Opt. Express*, 2018, **26**, 20319-20330.
18. D. Zhang, X. Ma, S. Wang and X. Zhu, *Plasma Science and Technology*, 2015, **17**, 971-974.
19. P. J. Skrodzki, N. Shah, N. Taylor, K. Hartig, N. LaHaye, B. Brumfield, I. Jovanovic, M. C. Phillips and S. S. Harilal, *Spectrochim. Acta B*, 2016, **125** 112–119.
20. X. L. Mao, G. C. Y. Chan, I. Choi, V. Zorba and R. E. Russo, *Journal of Radioanalytical and Nuclear Chemistry*, 2017, **312**, 121-131.
21. M. S. Finko and D. Curreli, *Physics of Plasmas*, 2018, **25**, 083112.
22. B. Koroglu, S. Wagnon, Z. R. Dai, J. C. Crowhurst, M. R. Armstrong, D. Weisz, M. Mehl, J. M. Zaug, H. B. Radousky and T. P. Rose, *Sci Rep-Uk*, 2018, **8**, 10451.
23. J. Serrano, J. Moros and J. J. Laserna, *Physical Chemistry Chemical Physics*, 2016, **18**, 2398-2408.
24. R. Glaus, J. Riedel and I. Gornushkin, *Analytical Chemistry*, 2015, **87**, 10131-10137.
25. S. Sreedhar, E. N. Rao, G. M. Kumar, S. P. Tewari and S. V. Rao, *Spectrochimica Acta Part B-Atomic Spectroscopy*, 2013, **87**, 121-129.
26. S. S. Harilal, B. E. Brumfield, B. Cannon and M. C. Phillips, *Anal. Chem.*, 2016, **88**, 2296-2302.
27. H.-J. Kunze, *Introduction to plasma spectroscopy*, Springer, Heidelburg, 2009.
28. S. A. Kalam, E. N. Rao and S. V. Rao, *Laser Focus World*, 2017, **53**, 24-28.
29. N. Farid, S. S. Harilal, H. Ding and A. Hassanein, *J. Appl. Phys.*, 2014, **115**, 033107.
30. G. C. Y. Chan, X. L. Mao, I. Choi, A. Sarkar, O. P. Lam, D. K. Shuh and R. E. Russo, *Spectrochimica Acta Part B-Atomic Spectroscopy*, 2013, **89**, 40-49.
31. A. Sarkar, D. Alamelu and S. K. Aggarwal, *Talanta*, 2009, **78**, 800-804.
32. E. J. Judge, J. E. Barefield, J. M. Berg, S. M. Clegg, G. J. Havrilla, V. M. Montoya, L. A. Le and L. N. Lopez, *Spectrochimica Acta Part B-Atomic Spectroscopy*, 2013, **83-84**, 28-36.
33. J. E. Barefield, E. J. Judge, K. R. Campbell, J. P. Colgan, D. P. Kilcrease, H. M. Johns, R. C. Wiens, R. E. McInroy, R. K. Martinez and S. M. Clegg, *Spectrochimica Acta Part B: Atomic Spectroscopy*, 2016, **120**, 1-8.
34. S. S. Harilal, B. E. Brumfield and M. C. Phillips, *Optics Letters*, 2018, **43**, 1055-1058.
35. J. Bergevin, T.-H. Wu, J. Yeak, B. E. Brumfield, S. S. Harilal, M. C. Phillips and R. J. Jones, *Nature Communications*, 2018, **9**, 1273.
36. M. C. Phillips, B. E. Brumfield, N. L. LaHaye, S. S. Harilal, K. C. Hartig and I. Jovanovic, *Scientific Reports*, 2017, **7**, 3784.
37. P. T. Rumsby and J. W. M. Paul, *Plasma Physics and Controlled Fusion*, 1974, **16**, 247-260.
38. K. Hartig, B. Brumfield, M. C. Phillips and S. S. Harilal, *Spectrochim. Acta B*, 2017, **135**, 54-62.
39. P. Hough, T. J. Kelly, C. Fallon, C. McLoughlin, P. Hayden, E. T. Kennedy, J. P. Mosnier, S. S. Harilal and J. T. Costello, *Measurement Science & Technology*, 2012, **23**, 125204.
40. S. Gurlui, M. Agop, P. Nica, M. Ziskind and C. Focsa, *Physical Review E*, 2008, **78**, 026405.
41. S. S. Harilal, C. V. Bindhu, M. S. Tillack, F. Najmabadi and A. C. Gaeris, *J. Appl. Phys.*, 2003, **93**, 2380-2388.
42. S. Amoruso, A. Sambri and X. Wang, *J Appl Phys*, 2006, **100**, 013302.
43. M. Jedyński, J. Hoffman, W. Mróz, Z. Szymański, Appl. Surf. Sci. 2008, **255** 2230-2236.

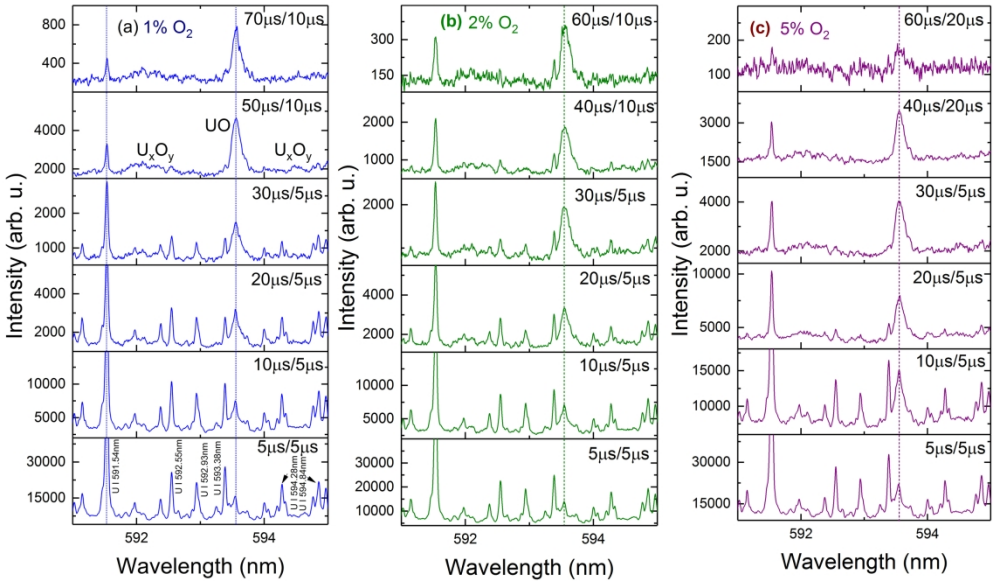

Figure 1: The time evolution of spectral emission from U plasma in the spectral range 591–595 nm at various oxygen partial pressures consists of emission from U I and UO: (a) 1% O_2 and, (b) 2% O_2 and (c) 5% O_2 partial pressures in 100 Torr Ar. The times given in each frame correspond to the time after the onset of plasma formation and gate width used for the measurement. The dotted lines given correspond to major U I and UO peaks.

234x135mm (300 x 300 DPI)

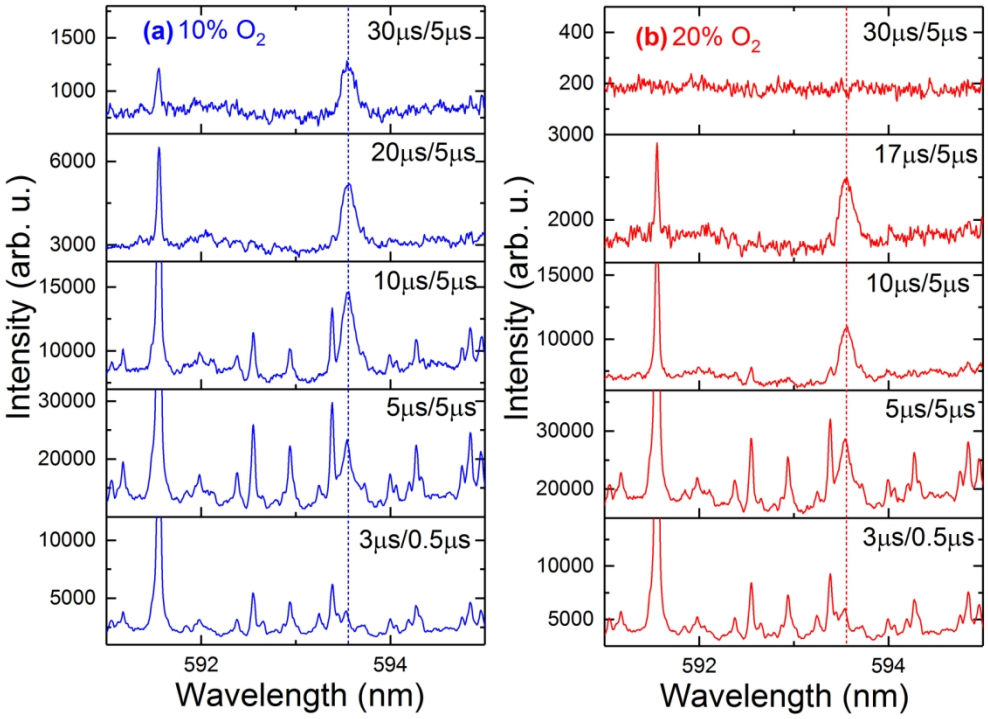

Figure 2: The temporal evolution of spectral emission from U plasma in the spectral range 591-595 nm with (a) 10% and (b) 20% oxygen PPs in 100 Torr Ar. The times given correspond to delay after the onset of plasma formation and gate width. The dotted lines given correspond to UO peak position.

155x110mm (300 x 300 DPI)

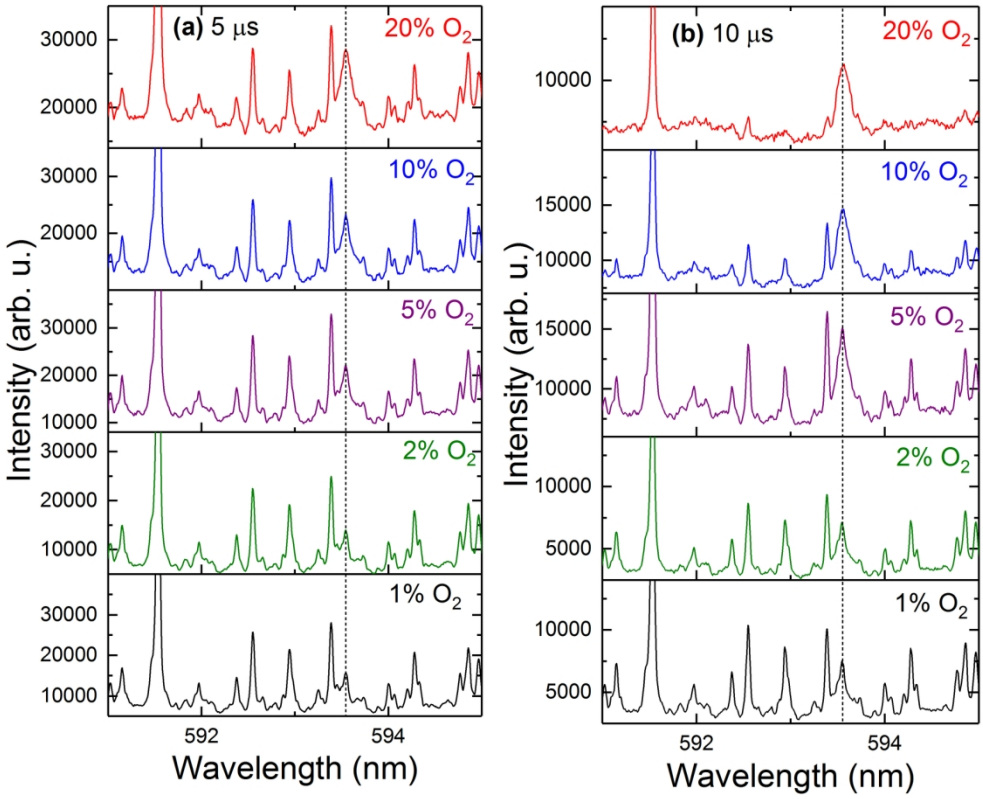

Figure 3: The spectral features recorded at various oxygen partial pressures for (a) 5 μs and (b) 10 μs. A 5 μs gate width is used for the measurement.

156x123mm (300 x 300 DPI)

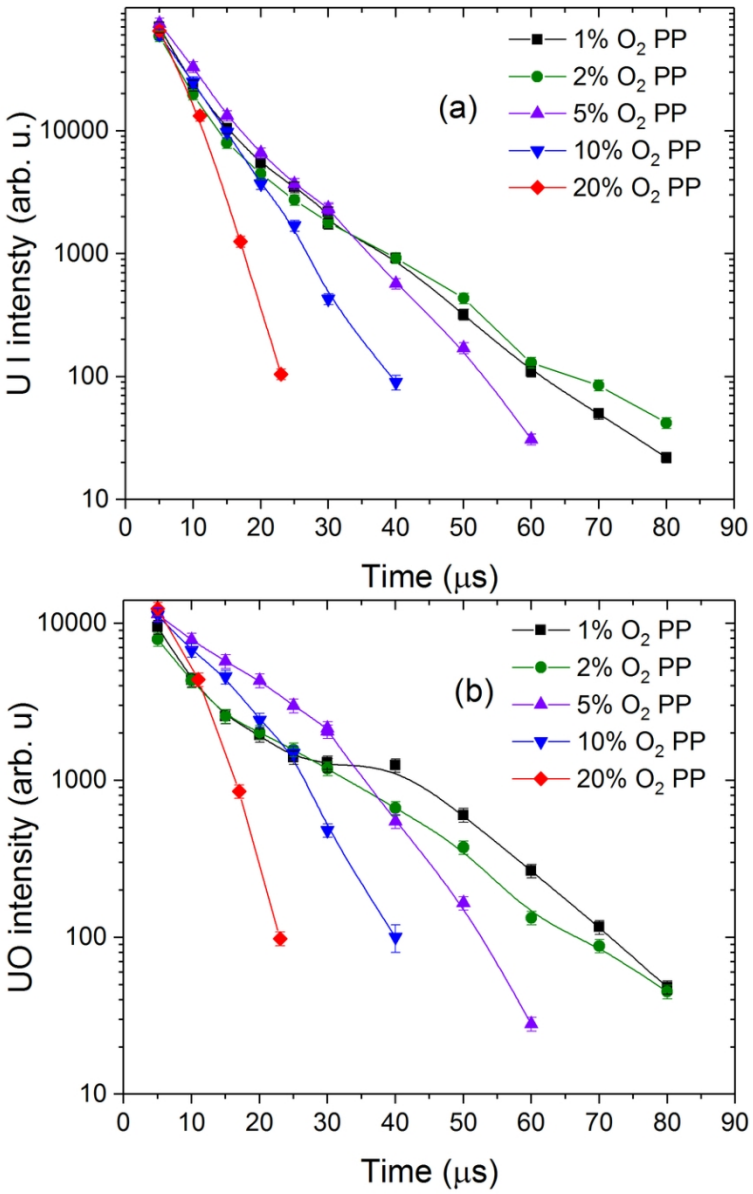

Figure 4: The peak intensities of (a) U I emission at 591.54 nm and (b) UO emission at 593.55 nm are given for various oxygen partial pressures.

76x121mm (300 x 300 DPI)

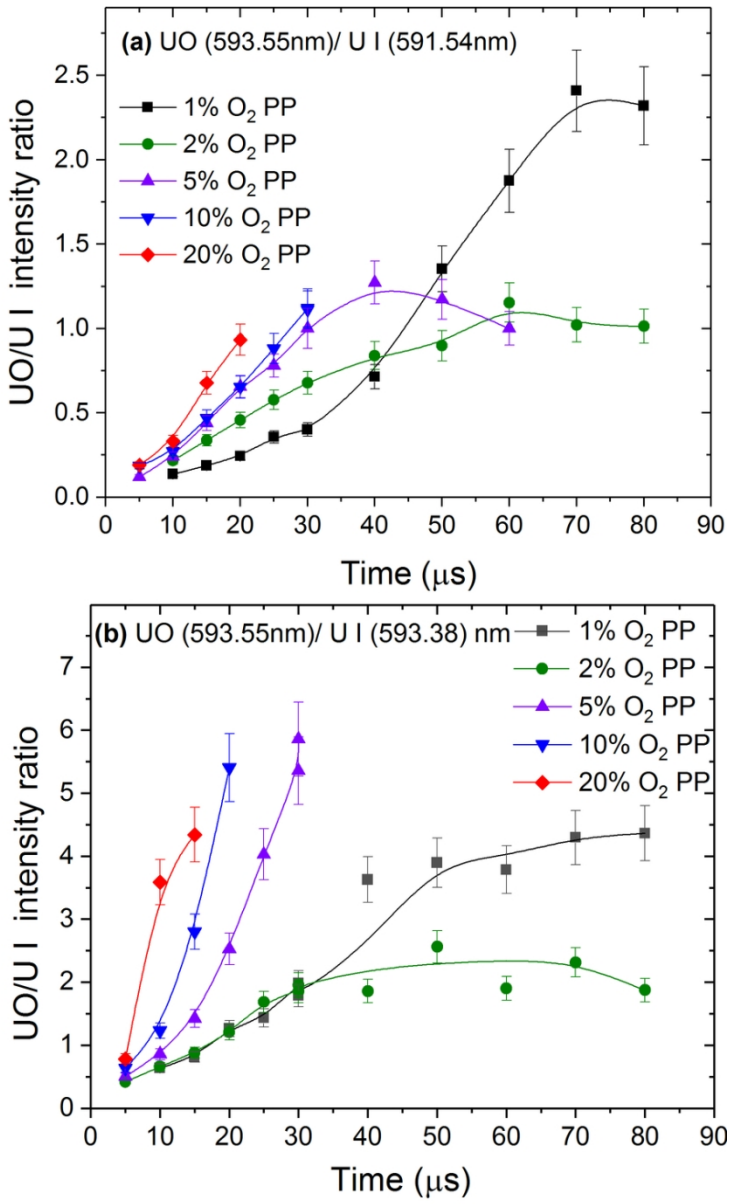

Figure 5: Time dependence of the ratio of UO/U I intensities for various $O_{2</sub}$ partial pressures at 100 Torr pressure. (a) The intensity ratio of UO 595.55 nm and U I 591.54 nm and (b) UO 593.55 nm to U 593.38 nm intensity ratio. The solid lines represent a guide to the eye.

76x125mm (300 x 300 DPI)

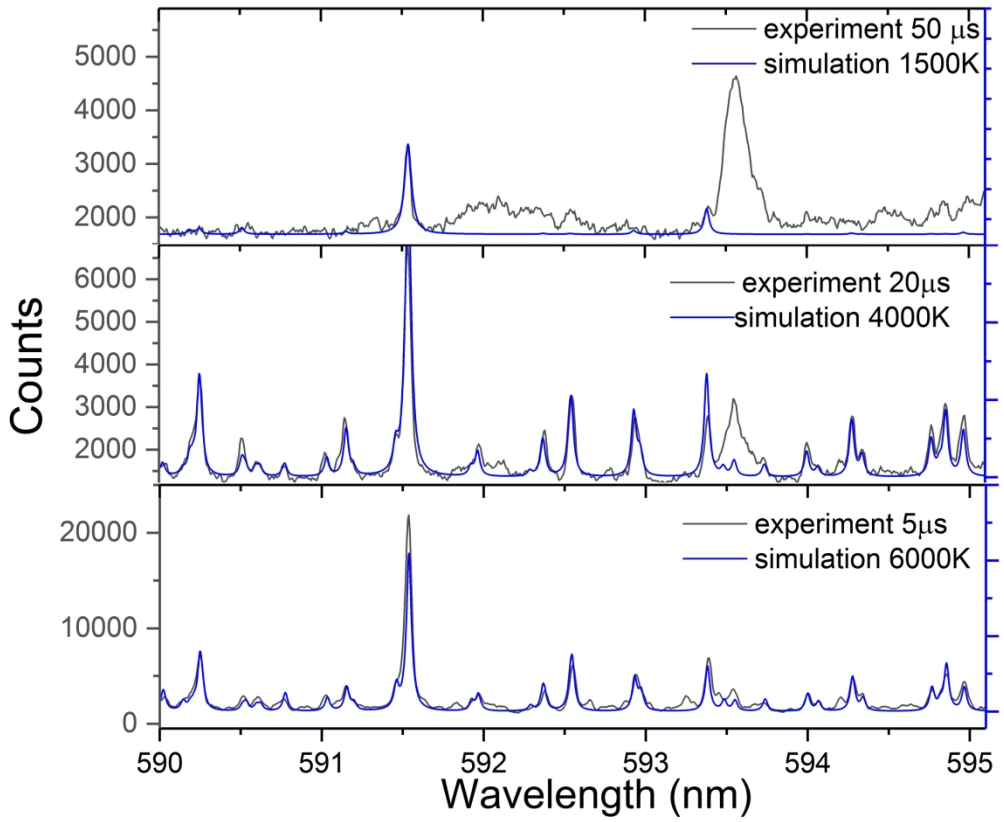

Figure 6: Time-resolved emission spectra of U plasma recorded with 1% O_2 PP (black) along with simulated spectra (blue) for various excitation temperatures.

224x185mm (300 x 300 DPI)

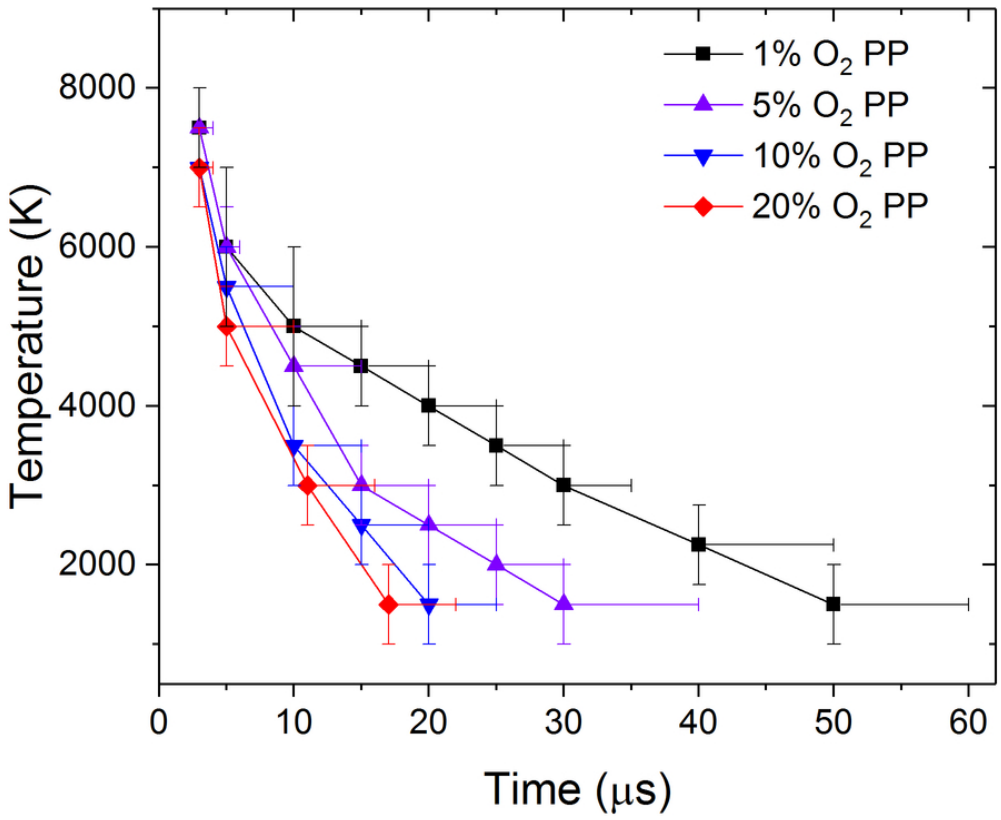

Figure 7: Excitation temperature as a function of time after the onset of plasma formation. The temperature is measured by comparing the recorded spectral features with simulated spectra under LTE. The x-axis error bars correspond to the gate width used for the experimental measurements.

76x61mm (300 x 300 DPI)

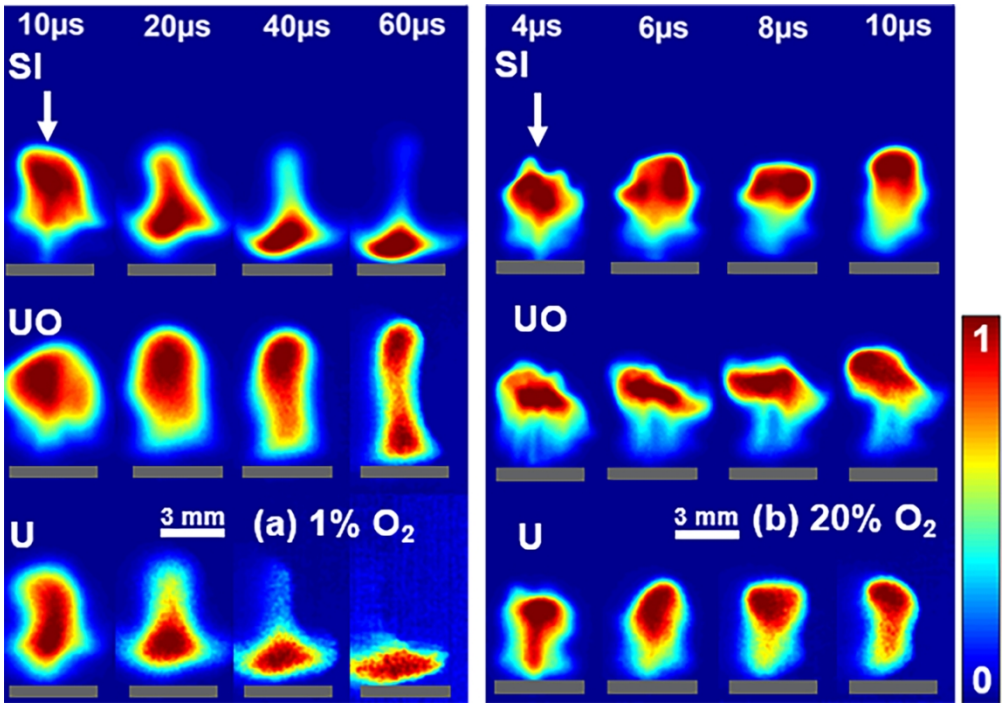

Figure 8: Time-resolved images of spectrally integrated (SI), UO, and U I (U) emission after the onset of plasma for (a) 1% O_2 and (b) 20% O_2 PPs. Integration time used were 1 µs for times until 10 µs, 5 µs for times between 10 and 30 µs and 10 µs for times 40 and 60 µs. Each image is obtained from a single shot event. The laser direction is marked with an arrow. The position of the target is given in each image.

109x76mm (300 x 300 DPI)

The complex interplay between plume hydrodynamics and chemistry impacts physical conditions leading to UO molecular formation in laser-plasmas.

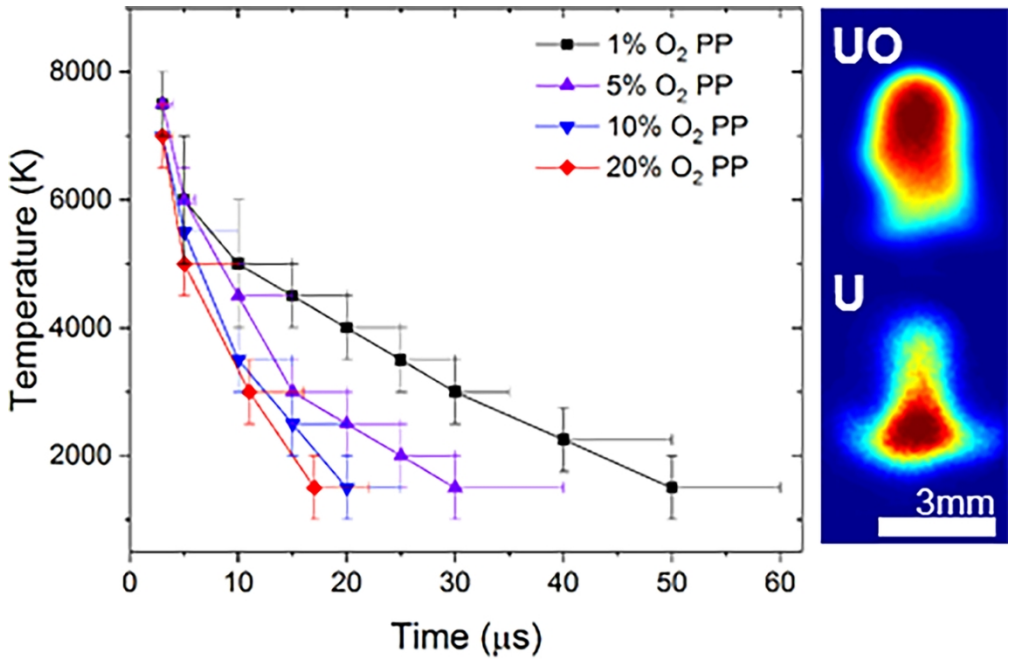

109x71mm (300 x 300 DPI)